Polarized hyper-Raman scattering study of the silent F_{2u} mode in $PbMg_{1/3}Nb_{2/3}O_3$

A. Al-Zein,[1,2] B. Hehlen,[1] J. Rouquette,[2] and J. Hlinka[3]
[1]*Laboratoire des Colloides, Verres et Nanomateriaux (LCVN), UMR CNRS 5587, University of Montpellier II, F-34095 Montpellier, France*
[2]*Institut Charles Gerhardt, UMR CNRS 5253, Equipe PMOF, University of Montpellier II, F-34095 Montpellier, France*
[3]*Institute of Physics, Academy of Sciences of the Czech Republic, Na Slovance 2, 18221 Praha 8, Czech Republic*
(Received 5 August 2008; revised manuscript received 4 October 2008; published 29 October 2008)

A single crystal of the relaxor $PbMg_{1/3}Nb_{2/3}O_3$ is studied by hyper-Raman scattering. The relative scattering intensities obtained for the band near 250 cm^{-1} in various polarization geometries are fully compatible with hyper-Raman spectroscopy tensor of the F_{2u} zone-center vibrational mode of prototype $Pm\bar{3}m$ (O_h^1) cubic perovskite structure. The mode was investigated between room temperature and 775 K, thus covering the range around the Burns temperature T_d and the crossover temperature T^*. At variance with recent anticipations, no softening was observed.

DOI: 10.1103/PhysRevB.78.134113 PACS number(s): 77.80.−e, 78.30.−j, 63.20.−e

I. INTRODUCTION

Hyper-Raman spectroscopy (HRS) is based on a nonlinear optical process where two incident photons produce one scattered photon after interaction with an elementary excitation in the material, such as long-wavelength optic phonon modes in crystals.[1] One of its big advantages in studying lattice dynamics is that selection rules for HRS differ from those for Raman scattering and infrared spectroscopies.[1,2] For example, the simple $Pm\bar{3}m$ parent cubic perovskite structure of ferroelectrics such as $BaTiO_3$ or $PbTiO_3$ has in total $3F_{1u}+1F_{2u}$ zone-center optic modes. It is well known that none of these species is allowed in first-order Raman spectra. Infrared spectroscopy allows one to study the F_{1u} modes but not the "silent" nonpolar F_{2u} mode. On the other hand, all of these modes are allowed by symmetry in first-order HRS.[3]

The average structure of the relaxor $PbMg_{1/3}Nb_{2/3}O_3$ (PMN) is exactly that of the paraelectric $BaTiO_3$. At the nanometer scale, the crystal structure of PMN is known to have a lower symmetry, for example, due to the short-range occupational ordering on the perovskite B site ($Fm\bar{3}m$-like clusters) and due to the short- or medium-range displacement order of ferroelectric type (polar nanoregions). These structural fluctuations are expected to modify the vibrational spectra. In the case of infrared reflectivity spectra, a splitting of the polar F_{1u} modes was observed and explained as due to the local dielectric anisotropy, most likely associated with local polar order.[4] In the case of Raman spectroscopy, both occupational and displacement short-range orders are often invoked to explain the first-order-like Raman spectra observed in this family of materials. However, Raman scattering in PMN does not show any clear-cut systematic extinction with respect to polarization analysis and the detailed assignment of the Raman bands thus remains an open problem.

In this situation, HRS provides a very interesting alternative with which to access the phonon spectra of lead-based relaxor materials. One of the most striking results of the few HRS experiments performed so far on mixed lead-based perovskites[3,5,6] is the dominant scattering by longitudinal-optic (LO) modes. These LO modes were particularly clearly seen in the HRS spectra of PMN.[6] Surprisingly, the ratios between the LO-mode strengths as observed in forward-scattering HRS spectra and the intensities of the corresponding bands in $-\mathrm{Im}[1/\epsilon]$ spectrum determined from far-infrared reflectivity spectra[4] were the same for the three main LO bands. This observation strongly indicates that the HRS intensity of LO modes comes from an electro-optic mechanism.[6] But details of this mechanism, which possibly may involve the nanoscale disorder, are not understood yet.

Another challenging opportunity is to investigate the silent F_{2u} mode, which should normally be active exclusively in HRS. Being a nonpolar mode, it has no LO-TO splitting and the electro-optic mechanism does not contribute to its strength in HRS spectra. In the course of our previous exploratory HRS study[6] of pure PMN, we indeed found a vibrational mode at a frequency near 250 cm^{-1} and with an intensity depolarization ratio that conforms to the F_{2u} symmetry. To confirm our assignment and verify the applicability of the symmetry selection rules, in the present study we have recorded a number of polarized HRS spectra in various geometries designed to probe independently phonon modes propagating along the [001], [110], and [111] crystallographic directions.

The F_{2u} mode is unique also in the sense that its eigenvector corresponds solely to the bending of oxygen octahedra.[3] Since no cation displacements are involved, eventual changes in its frequency with temperature or B-site substitutions have to be related to the change in force constants, as its eigenvector and effective mass remain preserved. Interestingly, recent HRS measurements in $Pb(Mg_{1/3}Nb_{2/3})_{0.73}Ti_{0.27}O_3$ (PMN-27PT) suggested that the F_{2u} mode might drastically soften[3] near $T_0=570$ K, which is close to the so-called Burns temperature T_d, below which the lattice parameter and refractive index deviate from the asymptotic linear behavior[7,8] and where the acoustic emission peak was observed.[8] It was then speculated that the competing F_{2u} order parameter can contribute to the suppression of long-range polar order in relaxors.[3] In fact, several authors have reported the existence of *two* distinct characteristic temperatures above the temperature of the dielectric

 ©2008 The American Physical Society

anomaly T_m in lead-based relaxors: T^* and T_d, which should be near about 350 and 620 K in PMN,[9] respectively, and near about 470–550 and 650–730 K, respectively, in a similar compound, $PbZn_{1/3}Nb_{2/3}O_3$.[10,11] Therefore, we have here carried out high-temperature measurements with the aim to follow the frequency of the F_{2u} vibrational mode in PMN up to the Burns temperature.

II. THEORETICAL BACKGROUND

The differential scattering cross section per unit volume S_{HR} for HRS by a phonon mode is, according to Ref. 12, given by

$$S_{\mathrm{HR}} = I_L \frac{2\pi}{c\sqrt{\epsilon_\infty}} \left(\frac{\omega_S}{c}\right)^4 \frac{V}{N} \frac{\hbar}{2\omega} [n(\omega)+1] F(\omega) R^2, \tag{1}$$

and

$$R^2 = \sum_\delta |e_i^S R_{ijk}^\delta e_j^L e_k^L|^2, \tag{2}$$

where I_L is the exciting laser intensity (power flux), N is the number of unit cells within the scattering volume V, ω_S is the outgoing-photon frequency, ω is the frequency shift related to the laser frequency ω_L through $\omega=2\omega_L-\omega_S$, $\sqrt{\epsilon_\infty}$ is the refractive index near ω_L, $n(\omega)$ stands for the Bose-Einstein population number, and $F(\omega)$ stands for a normalized response function of the phonon mode under consideration.

The factor R^2 expanded in Eq. (2) describes the dependence of S_{HR} on the scattering geometry defined by the Cartesian components of polarization vectors of the incident (L) and detected (S) photons, $\mathbf{e^L}$ and $\mathbf{e^S}$. The summation index δ distinguishes independent eigenvectors in the case of degenerate modes, and R_{ijk}^δ stands for the elements of the so-called HRS tensor of third rank associated with given phonons. In the case of O_h crystal symmetry, elements of the F_{1u}-mode HRS tensor can be written using the standard abbreviated notation ($a=R_{111}^x$, $b=R_{122}^x$, $b'=R_{212}^x$) as[12]

$$R^x(F_{1u}) = \begin{pmatrix} a & b & b & 0 & 0 & 0 \\ 0 & 0 & 0 & 0 & 0 & b' \\ 0 & 0 & 0 & 0 & b' & 0 \end{pmatrix},$$

$$R^y(F_{1u}) = \begin{pmatrix} 0 & 0 & 0 & 0 & 0 & b' \\ b & a & b & 0 & 0 & 0 \\ 0 & 0 & 0 & b' & 0 & 0 \end{pmatrix},$$

$$R^z(F_{1u}) = \begin{pmatrix} 0 & 0 & 0 & 0 & b' & 0 \\ 0 & 0 & 0 & b' & 0 & 0 \\ b & b & a & 0 & 0 & 0 \end{pmatrix}. \tag{3}$$

Similarly, the HRS tensor of the silent F_{2u} phonon mode reads ($c=R_{122}^x$, $c'=R_{212}^x$)

$$R^x(F_{2u}) = \begin{pmatrix} 0 & c & -c & 0 & 0 & 0 \\ 0 & 0 & 0 & 0 & 0 & c' \\ 0 & 0 & 0 & 0 & -c' & 0 \end{pmatrix},$$

$$R^y(F_{2u}) = \begin{pmatrix} 0 & 0 & 0 & 0 & 0 & -c' \\ -c & 0 & c & 0 & 0 & 0 \\ 0 & 0 & 0 & c' & 0 & 0 \end{pmatrix},$$

$$R^z(F_{2u}) = \begin{pmatrix} 0 & 0 & 0 & 0 & c' & 0 \\ 0 & 0 & 0 & -c' & 0 & 0 \\ c & -c & 0 & 0 & 0 & 0 \end{pmatrix}. \tag{4}$$

The Cartesian reference system assumed in Eqs. (3) and (4) is the one associated with the cubic crystallographic axes x, y, and z. Moreover the matrices R^x, R^y, and R^z in the case of the F_{1u} mode correspond to the components associated with dipolar moment along x, y, and z, respectively.[12] Due to the LO-TO splitting of F_{1u} polar modes, it is usually necessary to consider separately the tensors describing the LO mode and the tensors belonging to the TO-mode doublet. Corresponding tensors can be calculated from those of Eq. (3) using directional cosines of the phonon wave vector as it is described, for example, in Ref. 12.

Explicit values of the R^2 factor for the F_{1u} and F_{2u} modes in a range of scattering geometries accessible in our experimental conditions are summarized in Table I (part a). In order to describe the various scattering geometries, we use the usual Porto notation $a(bc)d$, where a and b stand for the incident-phonon propagation and polarization directions, and d and c stand for the outgoing-phonon propagation and polarization directions. High-symmetry axes exploited in the experiment are denoted as follows: $x\|[100]$, $y\|[010]$, $z\|[001]$, $x'\|[110]$, $y'\|[1\bar{1}0]$, $x''\|[11\bar{2}]$, and $z''\|[111]$.

In the usual case where electronic transition frequencies are high with respect to phonon and laser frequencies, HRS tensors are fully symmetric so that $b=b'$ and $c=c'$.[13] In this case, the expressions for R^2 reduce to those summarized in the last three columns of Table I (part b). For the sake of convenience, we tabulated the values normalized by $(R_{122}^x)^2/12$, denoting $\eta=a/b$ in the case of the F_{1u} tensor. In this case, the expected relative intensities in different geometries for a given species can be more easily appreciated. (It should be kept in mind here that a and b in the case of LO modes are different from those for TO modes due to the strong electro-optic contribution to LO-mode HRS tensors.)

III. EXPERIMENTAL

In this experiment we used commercially available PMN single crystals grown at Shanghai Institute of Ceramics. All samples were transparent, both-side polished, and were about 1-mm-thick plates of 7×7 mm^2. Crystallographic orientations of the direction normal to the surface in samples A, B, and C were (001), (110), and (111), respectively. Prior to the HRS experiments, the orientation of the crystallographic axes was verified on all samples by x-ray diffraction.

The HRS were measured with the same apparatus as used in our previous study.[6] The instrument uses a 2500 Hz pulsed yttrium aluminum garnet laser ($\lambda=1.064$ μm, $\sim$20 ns pulse width). The beam is focused to a $\sim$20-μm-diameter waist in the sample with the help of a $f=5$ cm lens. The incident peak power was kept slightly below the optical damage

TABLE I. HRS symmetry selection rules indicating normalized relative intensities of F_{1u} and F_{2u} modes in an O_h-symmetry crystal in various backscattering geometries. Part (a) describes the general conditions for first-order HRS. Part (b) gives results for the case of *fully symmetric* HRS tensors ($b=b'$ and $c=c'$) as a function of $\eta=a/b$.

	Scattering geometry		(a) General case			(b) Fully symmetric case		
Sample (**q**)	No.	Symbol	$R^2_{\mathrm{TO}}(F_{1u})$	$R^2_{\mathrm{LO}}(F_{1u})$	$R^2(F_{2u})$	$\frac{12}{b^2}R^2_{\mathrm{TO}}(F_{1u})$	$\frac{12}{b^2}R^2_{\mathrm{LO}}(F_{1u})$	$\frac{12}{c^2}R^2(F_{2u})$
A, **q**$\parallel$(001)	1	$z(xx)\bar{z}$	a^2	0	0	$12\eta^2$	0	0
	2	$z(x'x')\bar{z}$	$(\frac{a+b+2b'}{2})^2$	0	$\frac{1}{4}(c+2c')^2$	$27(1+\frac{\eta}{3})^2$	0	27
	3	$z(xy)\bar{z}$	b^2	0	c^2	12	0	12
	4	$z(x'y')\bar{z}$	$(\frac{a+b-2b'}{2})^2$	0	$\frac{1}{4}(c-2c')^2$	$3(1-\eta)^2$	0	3
B, **q**$\parallel$(110)	5	$x'(zz)\bar{x}'$	a^2	0	0	$12\eta^2$	0	0
	6	$x'(y'y')\bar{x}'$	$(\frac{a+b+2b'}{2})^2$	0	$\frac{1}{4}(c+2c')^2$	$27(1+\frac{\eta}{3})^2$	0	27
	7	$x'(zy')\bar{x}'$	b^2	0	c^2	12	0	12
	8	$x'(y'z)\bar{x}'$	b^2	0	0	12	0	0
C, **q**$\parallel$(111)	9	$z''(y'y')\bar{z}''$	$(\frac{a+b+2b'}{2})^2$	0	$\frac{1}{4}(c+2c')^2$	$27(1+\frac{\eta}{3})^2$	0	27
	10	$z''(x''x'')\bar{z}''$	$(\frac{a+b+2b'}{2})^2$	$\frac{1}{2}(\frac{a-b-2b'}{3})^2$	$\frac{1}{12}(c+2c')^2$	$27(1+\frac{\eta}{3})^2$	$6(1-\frac{\eta}{3})^2$	9
	11	$z''(y'x'')\bar{z}''$	$(\frac{a+5b-2b'}{6})^2$	$\frac{1}{2}(\frac{a-b-2b'}{3})^2$	$\frac{1}{12}(c+2c')^2$	$3(1+\frac{\eta}{3})^2$	$6(1-\frac{\eta}{3})^2$	1
	12	$z''(x''y')\bar{z}''$	$(\frac{a+5b-2b'}{6})^2$	0	$c'^2+\frac{c^2}{4}+\frac{cc'}{3}$	$3(1+\frac{\eta}{3})^2$	0	19

threshold, which for the present samples was about 2 kW. Backscattered photons were collected with a $f/1.5$ photo-objective lens, analyzed with a $f/5.6$ Jobin Yvon single 600-groove grating diffractometer and detected by nitrogen-cooled charge coupled device camera. High-temperature measurements were performed in a hot stage with temperature stabilization within about ± 1 K. The cooling and heating rates were about 10 K/min. Prior to any acquisition of the HRS spectra, the sample was stabilized at the required temperature for at least 10 min.

Our as-received samples exhibit a much larger hyper-Rayleigh scattering than that of the samples used in Ref. 6. This strong elastic line was filtered by a Notch filter of ~ 150 cm^{-1} half-width at half maximum. The HRS spectra were corrected by the transmission of the Notch, which was independently measured using a white-light source. This procedure allows reliable inelastic intensity measurements down to ~ 130 cm^{-1}. However, due to the very stiff increase in the transmission function, the elastic contribution can slightly change depending on the setting. This is the reason why we show the HRS intensities I_{HRS} without reduction by the Bose-Einstein factor. To get rid of the differences in the grating efficiency for light polarized parallel or perpendicular to the grooves, the polarization of the scattered light was analyzed using a broadband half-plate wave followed by a Glan-Thomson polarizer. Provided that the peaks are well defined, this optical setup allows polarization measurements with a precision greater than 1%. The quadratic dependence of the HRS process upon incident flux leads to a very tight definition of the scattering volume, in particular in the axial dimension (depth of field). This naturally produces a confocal-type effect in HRS and strongly favors the relative intensity measurements in samples of a good optical quality, as it was shown, e.g., in Refs. 14 and 15.

IV. RESULTS

A. HRS in various backscattering geometries

Figure 1 shows a set of polarized spectra obtained in various backscattering geometries using our three platelets A, B, and C, with the incident and scattered beams perpendicular to the large surface, hence probing phonons with a wave vector **q**$\parallel$(001), (110), and (111), respectively. For a given sample, it is also possible to change the orientation of the incident-light polarization with respect to the crystallographic axes by rotating the sample around **q**, e.g., by 45° for sample A and 90° for samples B and C. Consequently, four spectra per sample appear in Fig. 1. Sample B was measured immediately after sample A with the utmost care to maintain identical experimental conditions. Unfortunately, the orientation of the Notch filter was slightly changed for sample C, thus explaining the stronger elastic tail at low frequencies. However we estimate that the relative inelastic intensities are still accurate to better than $\sim 10\%$.

All the spectra exhibit quite strong peaks near 400 and 700 cm^{-1}, originating from the LO2 and LO3 modes, respectively. We note that, according to Table I, the LO modes should not appear in the spectra taken from samples A and B at all. The unusual behavior of LO modes appears to be a phenomenon inherent to HRS by PMN and related materials in general, and it was discussed in detail in Ref. 6. We have

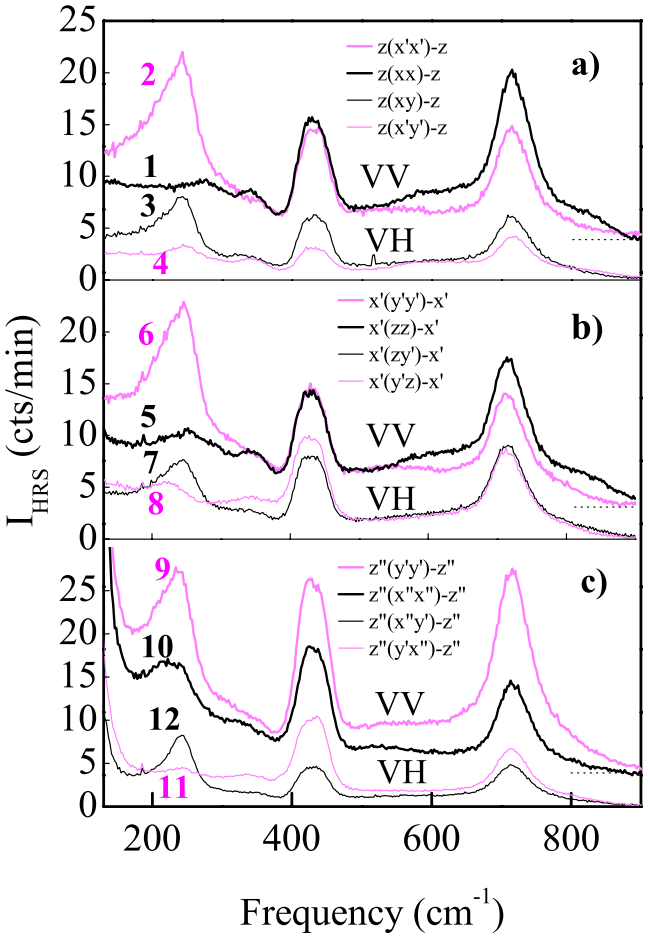

FIG. 1. (Color online) Room-temperature polarized HRS spectra in relative units taken in different backscattering geometries: (a) sample A with $\mathbf{q}\|(001)$, (b) sample B with $\mathbf{q}\|(110)$, and (c) sample C with $\mathbf{q}\|(111)$.

recently remarked that LO intensity in backscattering experiments decreases when the scattering volume (selected by the focusing geometry) approaches the front face of the crystal. This brought us to the conclusion that most of the LO-mode backscattering intensity may actually arise from events involving a near-forward HRS process (which is indeed very efficient for LO modes[6]) and reflection of the incident beam on the back face of the sample. However, the existence of an intrinsic phenomenon that would lift selection rules for HRS by LO modes cannot be definitely excluded.[6]

The F_{2u} vibrational mode is located[6] near 250 cm^{-1}, and it is clearly seen, e.g., in spectrum 2 in Fig. 1(a), corresponding to $z(x'x')\bar{z}$ geometry. The mode is also seen in $z(xy)\bar{z}$ (VH) spectrum 3 but not in the $z(xx)\bar{z}$ (VV) spectrum 1, in full agreement with the F_{2u} general selection rules shown in Table I. Such a complete extinction was not observed in our earlier study,[6] possibly due to some structural imperfections or the presence of differently oriented grains in the previously studied PMN crystal. The present experiment allows us to estimate even the relative intensities of the F_{2u} mode in different geometries. For example, the F_{2u} intensities in spectra 2 and 6 are almost equal, in agreement with Table I, and the same holds for spectra 3 and 7. Moreover, the ratio

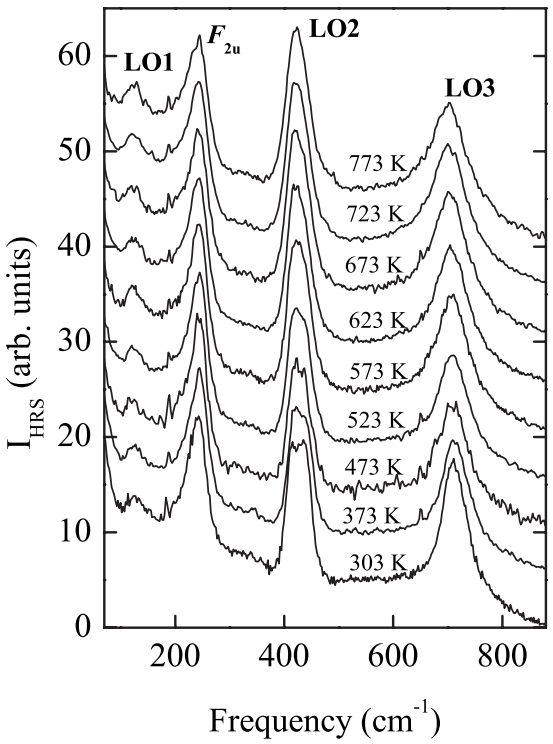

FIG. 2. HRS spectra of PMN taken in $z''(x''y')\bar{z}''$ geometry at various temperatures.

of the F_{2u} intensities in spectra 2 and 3 in Fig. 1(a) is slightly larger than 2, which implies that $c' \approx c$ (see Table I), i.e., that the usual case of a fully symmetric HRS tensor (last column of the Table I) seems to be relevant here.

In principle, the relations discussed so far would also hold true for TO modes of F_{1u} if by chance the absolute value of element a were much smaller than that of b ($\eta \approx 0$). Nevertheless, F_{1u}(TO) and F_{2u} modes can be distinguished with the help of spectrum 8. Indeed, according to Table I, the F_{1u}(TO)-mode intensity in spectrum 8 should be identical to that of spectra 3 and 7, while for the F_{2u} mode, no intensity is expected in spectrum 8. Thus, comparison of spectrum 8 with 7 or 3 confirms that the mode at 250 cm^{-1} is indeed the anticipated F_{2u} mode.

B. Temperature dependence of F_{2u} mode

For the high-temperature measurements, we selected the $z''(x''y')\bar{z}''$ (VH) geometry (sample C, spectrum 12) because, according to Table I (part b), the F_{2u} vs F_{1u}(TO) intensity ratio was expected to be sufficiently large to allow us to neglect the TO1 contributions there. Measurements were done in a single heating sequence. The spectra are shown in Fig. 2. In each spectrum, three LO bands and the F_{2u} band can be clearly seen. The splitting of LO2 seems to close at temperatures above T_d, which might indicate some change in the local polarization ordering. However, the F_{2u} mode does not appear to be affected by heating above the T^* and T_d at all.

The absence of the F_{2u}-mode softening toward the Burns temperature in PMN strongly indicates that the hypothetical

relation[3] between the softening of the F_{2u} mode and the Burns temperature is very unlikely. Indeed, the Burns temperature is known to be rather insensitive to the Ti content in PMN-PT compounds. So, in such a case, the same should hold for the F_{2u}-mode softening. Moreover, the F_{2u}-mode eigenvector involves only the bending vibrations of the oxygen skeleton. It also implies that the F_{2u}-mode frequency should not so drastically depend on the Ti content in PMN-PT compounds.

In fact, we rather expect that the analogous F_{2u} mode in PMN-27PT has almost identical frequency as in PMN crystal. If so, the soft modes observed in the HRS experiment on PMN-27PT (Ref. 3) do not correspond to the F_{2u} mode so far considered: either these soft modes are not F_{2u} modes at all or at least they have completely different eigenvectors. Therefore, it would be now highly interesting to analyze the low-frequency part of the HRS spectrum also in PMN, and check if the polarization selection rules for these soft modes are actually those of F_{2u} symmetry or not. Preliminary experiments indicate that low-frequency soft modes as reported in PMN-27PT are indeed possible to detect in PMN with our experimental setup and a detailed study is currently in progress.

V. DISCUSSION

The spectra shown in Fig. 1 show some other features not discussed so far. For example, spectra 1 and 5 have a pronounced peak near 340 cm^{-1} that we have earlier[4,6,16] assigned to the fourth F_{1u} mode of the $Fm\bar{3}m$ clusters of partial 1:1 occupational order on B sites, deduced from (1/2 1/2 1/2) diffuse reflections in diffraction experiments. This mode primarily corresponds to the antiparallel vibrations of neighboring B-site cations (B-B beating).[16,17] The LO-TO splitting of this weak B-B mode is certainly small with respect to the apparent width. From the comparison of B-B vs LO2 relative intensity in our HRS and in $\mathrm{Im}[1/\epsilon]$ spectra from Ref. 4, we infer that the B-B mode contributes here mainly through its anomalously scattering LO component.

Spectra 1 and 5 show also broad features near 800, 550, and 270 cm^{-1}, which are rather close to the main bands observed in Raman scattering.[9,18–23] Such "background" spectra could eventually arise from a Raman scattering generated by the second-harmonic signal, similarly as it was observed, for example, in PZT.[5] However, a calibration of the Raman and hyper-Raman relative intensities reveals that in our PMN samples, such a contamination should not exceed 0.2 counts/min (at frequencies of the main Raman bands) and it means that it is negligible in the HRS spectra shown here. However, since there are no first-order Raman-active modes in PMN except for those activated by short-range order, the shape of the Raman spectra of PMN can be probably understood as originating from a weighted phonon density of states. Obviously, the same short-range order may in principle introduce a similar density-of-states-like component in the HRS spectra.

On top of these contributions, one should expect HRS by the principal F_{1u}(TO) modes. Judging from the corresponding spectrum of $\mathrm{Im}[\epsilon]$ obtained from IR spectroscopy,[4] one can expect a strong scattering by a soft TO1 mode below 100 cm^{-1} (region inaccessible in this experiment), a TO2 band located near 225 cm^{-1}, and a weak TO3 band located near 550 cm^{-1}. Based on this correspondence, we expect that the weak mode observed near 225 cm^{-1} in spectrum 8 in Fig. 1(b) is actually due to the TO2 mode.

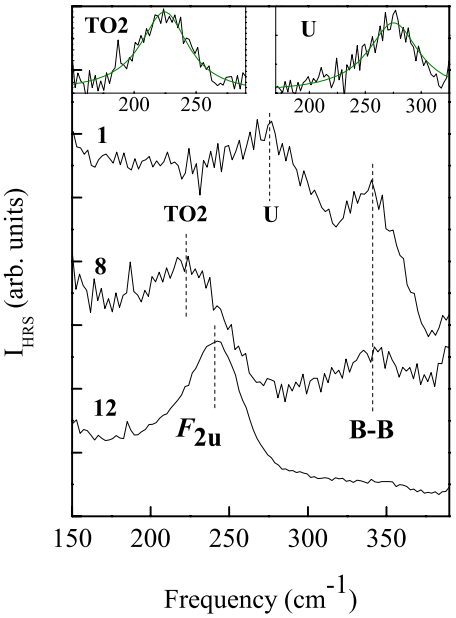

FIG. 3. (Color online) Details of HRS spectra 1, 8, and 12 from Fig. 1 in the spectral region around the F_{2u} band. Insets show DHO fits of TO2 and U bands after subtraction of the background signal.

In summary, it seems that the F_{2u} band in spectra in Fig. 1 more or less overlaps with two other different bands: the TO2 band at 225 cm^{-1} and the so far unassigned band U at 275 cm^{-1}. Therefore, a simple fitting procedure was applied here in order to get more quantitative information about these contributions. At first we have considered only spectra 1, 8, and 12, where these three bands seems to contribute rather separately (see Fig. 3), in order to extract their individual spectral responses. The fitting function has the form of a damped-harmonic-oscillator (DHO) response multiplied by the Bose-Einstein factor,

$$I(\omega) = I_0 \frac{\Gamma \omega \omega_0^2}{(\omega^2 - \omega_0^2)^2 + \Gamma^2 \omega_0^2}[n(\omega) + 1], \tag{5}$$

and a straight-line sloping background. The good fitting agreement for TO2 and U bands is shown in the insets of Fig. 3.

For the F_{2u} band shown in spectrum 12 in Fig. 3, a single DHO formula could not reproduce its asymmetric spectral line shape, so we have rather used the Breit-Wigner-Fano (BWF) formula[24,25]

$$I_{F_{2u}}(\omega) = I_0 \frac{\left(1 + \frac{\omega - \omega_0}{\alpha\gamma}\right)^2}{1 + \left(\frac{\omega - \omega_0}{\gamma}\right)^2}[n(\omega) + 1], \tag{6}$$

where ω_0 is the peak frequency, I_0 is its intensity, and α is a coefficient that relates to the degree of asymmetry of the line

TABLE II. Values of frequencies ω_0 and damping parameters Γ [defined in Eq. (5) and, in the case of F_{2u} mode, in Eq. (6)], as obtained from fits to data shown in Fig. 3.

	TO2	U	F_{2u}	*B-B*
ω_0 (cm^{-1})	224	274	247	340
Γ (cm^{-1})	47	55.3	40	47.1

(when $1/\alpha \to 0$, the profile reduces to a simple Lorentzian with a full width at half maximum $\Gamma = 2\gamma$). The fitting results for the position and linewidth of the TO2, U, and F_{2u}, as well as for the nearby *B-B* vibration, are displayed in Table II.

The asymmetric shape of F_{2u} may originate from inhomogeneous broadening, for example, due to the *B*-site disorder, which certainly modifies the stiffness of the inequivalent oxygen octahedra. However, the apparent asymmetry can be also effectively increased by the contribution of TO2 mode. Indeed, even in spectrum 12, where the F_{2u} band clearly exhibits the weakest apparent width, a small but finite contribution of the TO2 mode is expected according to Table I. Therefore, in the second step all spectra were adjusted to a linear combination of the same DHO and BWF functions, with their widths and frequencies fixed according to Table II, thus leaving adjustable only the individual intensities and the asymmetry parameter α. It turned out that all spectra could be adjusted in this way using $\alpha \simeq 7 \pm 2$.

The good quality of such fits for several representative spectra are shown in Fig. 4. For those, the U component around 274 cm^{-1} appears very weak relative to the F_{2u} band, so the fits only account for the F_{1u}(TO2) and F_{2u} vibrations. Resulting mode intensities can be scaled by a common factor in order to facilitate comparison with the numbers given in Table I. Normalization of the F_{2u} intensity from the fit to the $z''(x''y')\bar{z}''$ spectrum to the value of 19 gave values of 14 ± 1.5 and 6.7 ± 1 for the F_{2u} intensities in spectra 3 and 10 [$z(xy)\bar{z}$ and $z''(x''x'')\bar{z}''$], respectively. These numbers are in reasonably good agreement with those derived in the third and tenth lines of Table I (part b), emphasizing that the F_{2u} mode rather follows the selection rules for a fully symmetric HRS cubic tensor ($c = c'$). Similarly, the normalization of the F_{1u}(TO2) intensity in spectrum 10 [$z''(x''x'')\bar{z}''$] to the value of 27 leads to values of 11.6 ± 4 and 3 ± 3 for spectra 3 and 12 [$z(xy)\bar{z}$ and $z''(x''y')\bar{z}''$], respectively. These numbers are also in good agreement with the predictions in Table I for any reasonably small value of η. Thus, these results support our assignment of the 225 cm^{-1} band to an F_{1u}(TO) vibration. In principle, η^2 can be evaluated, for example, from the experimental ratio $I_{z(xx)\bar{z}}/I_{z(xy)\bar{z}}$. Our data indicate that η is probably smaller than 1/5; i.e., $b > 5a$ for the TO2 mode.

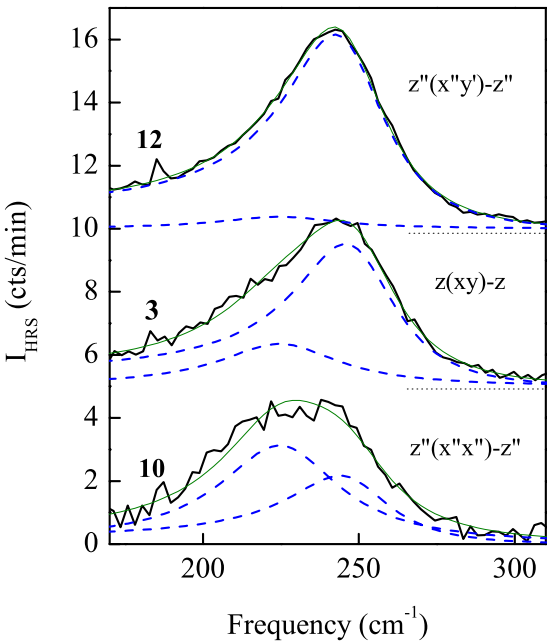

FIG. 4. (Color online) Adjustments of the selected room-temperature spectra in the vicinity of the F_{2u} band to a superposition of predefined TO2- and F_{2u}-band profiles, as explained in the text. For clarity, the background was removed and the spectra denoted 12 and 3 were translated vertically by 10 and 5 intensity units, respectively. Dashed lines show individual components corresponding to TO2 and the F_{2u} vibrations. The thin full line is the resulting fit.

VI. CONCLUSION

In conclusion, we have derived tables of relative HRS intensities in a number of high-symmetry backscattering geometries for the HRS-active optic modes of the $Pm\bar{3}m$ (O_h^1) cubic perovskites. By performing a corresponding set of HRS experiments on high-quality PMN single crystals, it was found that the 250 cm^{-1} band fully obeys the symmetry requirements for the silent F_{2u} vibration, and that its HRS tensor is at least approximately symmetric. The spectral line shape of the F_{2u} mode was found to be slightly asymmetric, with BWF asymmetric parameter of about 7 and damping parameter of about 40 cm^{-1} at room temperature. The crystal was heated well above the Burns temperature but no significant changes in the F_{2u} mode behavior were observed. In addition, several other modes were characterized. In particular, the F_{1u}(TO2) band near 225 cm^{-1} was also found to show good agreement with the predicted HRS intensity ratios for different scattering geometries.

In general, sufficiently small structural inhomogeneities are not expected to alter significantly the scattering intensity ratios for the regular zone-center optic modes of the average structure. These conditions are experimentally verified in the present case for both the F_{2u} and F_{1u}(TO2) modes of the relaxor PMN. Thus, we can conclude that HRS is a promising tool for studying the $Pm\bar{3}m$ (O_h^1) zone-center modes in weakly disordered complex cubic perovskites, including lead-based relaxors.

ACKNOWLEDGMENTS

This work was partly supported by the Grant Agency of the Czech Republic (Project No. 202/06/0411) and by the Czech Academy of Sciences (Project No. AV0Z10100520).

[1] V. N. Denisov, B. N. Marvin, and V. B. Podobedov, Phys. Rep. **151**, 1 (1987).
[2] S. J. Cyvin, J. E. Rauch, and J. C. Decius, J. Chem. Phys. **43**, 4083 (1965).
[3] H. Hellwig, A. Sehirlioglu, D. A. Payne, and P. Han, Phys. Rev. B **73**, 094126 (2006).
[4] J. Hlinka, T. Ostapchuk, D. Noujni, S. Kamba, and J. Petzelt, Phys. Rev. Lett. **96**, 027601 (2006).
[5] H. Hellwig, Appl. Phys. Lett. **87**, 051104 (2005).
[6] B. Hehlen, G. Simon, and J. Hlinka, Phys. Rev. B **75**, 052104 (2007).
[7] G. Burns and B. A. Scott, Solid State Commun. **13**, 423 (1973); G. Burns and F. H. Dacol, *ibid.* **48**, 853 (1983).
[8] E. Dul'kin, I. P. Raevskii, and S. M. Emel'yanov, Phys. Solid State **45**, 158 (2003).
[9] O. Svitelskiy, J. Toulouse, G. Yong, and Z.-G. Ye, Phys. Rev. B **68**, 104107 (2003).
[10] J.-H. Ko, D. H. Kim, and S. Kojima, Phys. Rev. B **77**, 104110 (2008).
[11] J. Toulouse, F. Jiang, O. Svitelskiy, W. Chen, and Z.-G. Ye, Phys. Rev. B **72**, 184106 (2005).
[12] H. Vogt, Phys. Rev. B **38**, 5699 (1988).
[13] H. Vogt, Phys. Rev. B **36**, 5001 (1987).
[14] G. Simon, B. Hehlen, R. Vacher, and E. Courtens, J. Phys.: Condens. Matter **20**, 155103 (2008).
[15] G. Simon, B. Hehlen, R. Vacher, and E. Courtens, Phys. Rev. B **76**, 054210 (2007).
[16] J. Hlinka, J. Petzelt, S. Kamba, D. Noujni, and T. Ostapchuk, Phase Transitions **79**, 41 (2006).
[17] I. M. Reaney, J. Petzelt, V. V. Voitsekhovskii, F. Chu, and N. Setter, J. Appl. Phys. **76**, 2086 (1994).
[18] M. El. Marssi, R. Farhi, and Yu. Yuzyuk, J. Phys.: Condens. Matter **10**, 9161 (1998).
[19] S. G. Lushnikov, S. N. Gvasaliya, and I. G. Siny, Physica B (Amsterdam) **263-264**, 286 (1999).
[20] F. Jiang, S. Kojima, Ch. Zhao, and Ch. Feng, J. Appl. Phys. **88**, 3608 (2000).
[21] H. Ohwa, M. Iwata, H. Orihara, N. Yasuda, and Y. Ishibashi, J. Phys. Soc. Jpn. **70**, 3149 (2001).
[22] S. A. Prosandeev, E. Cockayne, B. P. Burton, S. Kamba, J. Petzelt, Yu. Yuzyuk, R. S. Katiyar, and S. B. Vakhrushev, Phys. Rev. B **70**, 134110 (2004).
[23] A. Slodczyk, P. Daniel, and A. Kania, Phys. Rev. B **77**, 184114 (2008).
[24] J. F. Scott, Rev. Mod. Phys. **46**, 83 (1974).
[25] M. R. Dresselhaus and G. Dresselhaus, Adv. Phys. **30**, 139 (1981).